

# Quasiparticle and excitonic structures of few-layer and bulk GaSe: Interlayer coupling, self-energy, and electron-hole interaction

Fanhao Jia<sup>1,2,†</sup>, Zhao Tang<sup>1,3,4,‡</sup>, Greis J. Cruz,<sup>3</sup> Weiwei Gao<sup>5</sup>, Shaowen Xu,<sup>2</sup> Wei Ren,<sup>2,\*</sup> and Peihong Zhang<sup>1,3,†</sup>

<sup>1</sup>Department of Physics, Hangzhou Dianzi University, Hangzhou 310018, China

<sup>2</sup>International Centre of Quantum and Molecular Structures, Department of Physics, Shanghai University, Shanghai 200444, China

<sup>3</sup>Department of Physics, University at Buffalo, State University of New York, Buffalo, New York 14260, USA

<sup>4</sup>Center for Computational Materials, Oden Institute for Computational Engineering and Sciences, The University of Texas at Austin, Austin, Texas 78712, USA

<sup>5</sup>Key Laboratory of Material Modification by Laser, Ion, and Electron Beams, Dalian University of Technology, Ministry of Education, Dalian 116024, China

(Received 29 January 2024; revised 15 April 2024; accepted 18 April 2024; published 8 May 2024; corrected 21 January 2025)

Metal monochalcogenide GaSe is a classic layered semiconductor that has received increasing research interest due to its highly tunable electronic and optical properties for ultrathin electronics applications. Despite intense research efforts, a systematic understanding of the layer-dependent electronic and optical properties of GaSe remains to be established, and there appear to be significant discrepancies between different experiments. We have performed *GW* plus Bethe-Salpeter equation calculations for few-layer and bulk GaSe, aiming at understanding the effects of interlayer coupling and dielectric screening on excited-state properties of GaSe, and how the electronic and optical properties evolve from strongly two-dimensional-like to intermediate thick layers, and to three-dimensional bulk character. Using a new definition of the exciton binding energy, we are able to calculate the binding energies of all excitonic states. Our results reveal an interesting correlation between the binding energy of an exciton and the spread of its wave function in real and momentum spaces. We find that the existence of (nearly) parallel valence and conduction bands facilitates the formation of excitonic states that spread out in momentum space. Thus, these excitons tend to be more localized in real space and have large exciton binding energies. The interlayer coupling substantially suppresses the Mexican-hat-like dispersion of the top valence band seen in the monolayer system, explaining the greatly enhanced photoluminescence as layer thickness increases. Our results also help resolve apparent discrepancies between different experiments. After including the quasiparticle and excitonic effects as well as the optical activities of excitons, our results compare well with available experimental results.

DOI: 10.1103/PhysRevApplied.21.054019

## I. INTRODUCTION

Gallium selenide (GaSe) belongs to a large family of post-transition-metal monochalcogenide semiconductors [1–3] that has emerged as an important class of layered materials for applications ranging from ultrathin optoelectronics [4,5] to photocatalysis. Bulk GaSe has an optical band gap of around 2 eV at room temperature (around 2.1 eV at 10 K) [6–8]. Unlike monolayer transition-metal dichalcogenides such as MoS<sub>2</sub>, which has a direct band

gap, monolayer GaSe has an indirect band gap. Interestingly, the nature of the band gap (i.e., direct or indirect) of bulk GaSe is still not settled (we will discuss this issue later). The band dispersion near the valence band maximum (VBM) of few-layer GaSe also has an interesting Mexican-hat-like (MH-like) shape [5,9,10], with the VBM slightly shifted from the  $\Gamma$  point, while the conduction band minimum (CBM) is always at the  $\Gamma$  point.

It is well known that the band gaps (both quasiparticle and optical) of layered materials often increase significantly as the number of layers decreases due to quantum confinement, reduced interlayer coupling, and dielectric screening effects. For example, it was reported that the energy of the photoluminescence (PL) *A* peak of InSe increases from 1.27 eV for the bulk phase to 1.88 eV

\*Corresponding author: renwei@shu.edu.cn

†Corresponding author: pzhang3@buffalo.edu

‡FJ and ZT contributed equally to this work.

(bilayer) and 2.60 eV (monolayer) [11], suggesting the optical gap can be widely tuned by controlling the layer thickness. GaSe is expected to have similar tunability. However, experimental reports have yielded seemingly inconsistent findings. Earlier experiments suggested that the optical band gap of GaSe does not depend sensitively on the layer thickness [3,12,13]. More recent experiments, on the other hand, have observed significant layer dependence of the PL spectra. The peak position increased from 1.99 eV (bulk) to 2.42 eV (bilayer), and no PL peaks were observed for the monolayer system [14]. Cathodoluminescence (CL) experiments, in contrast, show a broad peak at about 3.3 eV [15] for monolayer GaSe. Quasiparticle (QP) band gaps measured by scanning tunneling spectroscopy (STS) are 3.5, 3.0, and 2.3 eV for monolayer, bilayer, and trilayer GaSe, respectively [16]. Therefore, there appear to be significant discrepancies between experiments.

In this work, we carried out accurate many-body perturbation theory (MBPT) calculations within the *GW* plus Bethe-Salpeter equation (BSE) approach [17,18] to understand the QP and optical properties of bulk and few-layer GaSe. The *GW* method is one of the most accurate methods for calculating QP excitations, whereas the excitonic and optical properties can be predicted by solving the BSE. We found that, even in this moderate-gap material, some above-gap bulk exciton states can be highly localized and have surprisingly large binding energies (as large as 168 meV) thanks to several pairs of nearly parallel valence and conduction bands in a portion of the Brillouin zone (BZ), which lead to delocalization of the exciton wave functions in *k* space and localization in real space. The calculated exciton binding energy of the lowest excitonic state of bulk GaSe, after extrapolating to the converged value, agrees very well with the experimental result. The unique excitonic structures and exciton binding energies of these systems are analyzed in detail to illustrate the effects of interlayer coupling and layer-dependent dielectric screening on excited-state properties of GaSe. Our work also helps reconcile the seemingly inconsistent experimental results.

## II. COMPUTATIONAL DETAILS

The structures of few-layer and bulk GaSe were optimized using the meta-generalized gradient approximation within the strongly constrained and appropriately normed (SCAN) functional plus revised Vydrov-van Voorhis nonlocal correlation *rVV10* [19], implemented in the Vienna *ab initio* simulation package (VASP) [20]. The SCAN+*rVV10* functional has been shown to accurately predict the structural properties of a range of layered materials [19]. A 25-Å vacuum slab was added in few-layer systems and a slab-truncated Coulomb potential [21] was used to minimize the interaction between periodic adjacent layers.

We used a local version of the BerkeleyGW code [22] to perform the *GW* [17] and BSE [18] calculations. The recently developed acceleration methods [23–26] were used for the *GW* calculations. These methods lead to a combined speed-up factor of up to 1000 for *GW* calculations for two-dimensional (2D) materials compared with conventional band-by-band summation and uniform *k*-point sampling approaches. The Hybertsen-Louie generalized plasmon-pole (HL GPP) model [17] was used to extend the static dielectric function to finite frequencies. The density-functional theory (DFT) part of the MBPT calculation was carried out using the Perdew-Burke-Ernzerhof (PBE) [27] functional and the Troullier-Martins norm-conserving pseudopotentials [28]. A plane-wave cut-off energy of 60 Ry was used in the DFT calculations, and we used a high cutoff energy of 30 Ry for the dielectric matrices and the *e-h* kernel in the *GW* and BSE calculations.

A dual-grid method [18] was applied to reduce the workload of the BSE calculations. For the few-layer systems, the *e-h* kernel was first calculated on an  $18 \times 18 \times 1$  coarse *k* grid; the results were then interpolated onto a finer grid ( $96 \times 96 \times 1$  for the monolayer,  $90 \times 90 \times 1$  for the bilayer, and  $78 \times 78 \times 1$  for the trilayer) while solving the BSE for the excitonic and optical properties. For the bulk system (which has a rather thick unit cell, as we will discuss later), the *e-h* kernel was calculated on a  $12 \times 12 \times 2$  *k* grid, which was then interpolated onto a  $36 \times 36 \times 8$  fine grid in solving the BSE. We have carefully checked the convergence of our *GW* and BSE results; see the Supplemental Material at [29] Fig. S1 for the details of the convergence tests.

## III. RESULTS AND DISCUSSION

### A. Structural properties of few-layer and bulk GaSe

Bulk GaSe exhibits several polymorphic modifications with different stacking and numbers of layers, while the  $\varepsilon$ -GaSe polytype (space group of  $P\bar{6}m2$ ) is the most common phase at room temperature [30]. The structure  $\varepsilon$ -GaSe consists of two hexagonal layers (Fig. 1) with Ga assuming a tetrahedral coordination and Se forming three covalent bonds with Ga. The hexagonal layer, although consisting of multiple atomic planes, is tightly bonded; therefore, it is considered to be a single layer (monolayer) in our study (with a layer thickness  $d_1$  as shown in Fig. 1). We assume the  $\varepsilon$ -like stacking in our study of few-layer and bulk GaSe, as shown in Fig. 1.

Table I compares the optimized structure of few-layer GaSe and the experimental structure of bulk GaSe [31]. The optimized lattice constant  $a$  and layer thickness  $d_1$  (defined in Fig. 1) of the few-layer systems show little change with the increasing number of layers and are very close to the experimental values (within 0.5%), suggesting the accuracy of the theory and the weak interlayer coupling

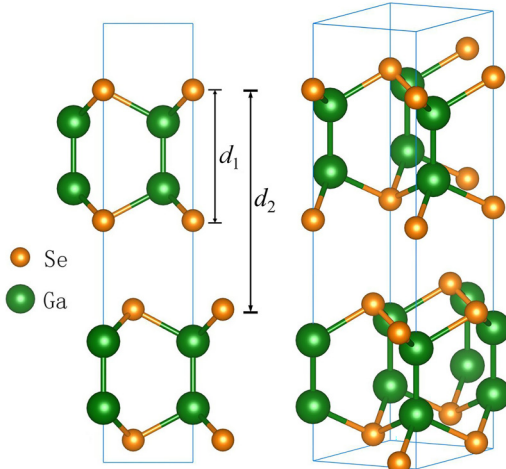


FIG. 1. Side view (left) and orthographic view (right) of the  $\epsilon$ -phase bulk GaSe.

effects on the structural properties. The  $d_2$  parameter is  $d_1$  plus the interlayer spacing (see Fig. 1).

## B. Quasiparticle band structures

Figure 2 compares the DFT and QP band structures of bulk and few-layer GaSe. Except for the band gap enlarging, the quasiparticle corrections do not seem to change the band dispersion significantly for bulk and few-layer systems. While few-layer systems have an indirect gap, bulk GaSe has a direct gap at  $\Gamma$ ; these results are consistent with previous calculations [32–36]. However, it should be mentioned that the nature of the band gap of bulk GaSe is still not fully settled. Experiments [37–39] seem to consistently indicate that bulk GaSe has an indirect band gap with the CBM located at the  $M$  point. However, there is also significant variation (25–500 meV) [37–39] in the energy difference ( $\Delta_{\Gamma M} = E_{\Gamma} - E_M$ ) between the  $\Gamma$  and the  $M$  points. In particular, Coletti *et al.* [38] observed that  $\Delta_{\Gamma M}$  decreases significantly with decreasing electron current. Since carriers are inevitably introduced in experiment, it is plausible the discrepancy between theory and experiment may be (at least partially) resolved by considering the carriers' renormalization effects. This issue deserves further investigation.

TABLE I. Lattice parameters (in angstroms) of few-layer and bulk GaSe used in this study. The values for few-layer systems are calculated using the SCAN +  $rVV10$  functional, while those of the bulk phase are taken from experiments [31].

	Monolayer	Bilayer	Trilayer	Bulk (exp)
$a$ (Å)	3.740	3.744	3.744	3.743
$d_1$ (Å)	4.768	4.768	4.762	4.776
$d_2$ (Å)		8.045	8.021	7.960 (= $c/2$ )

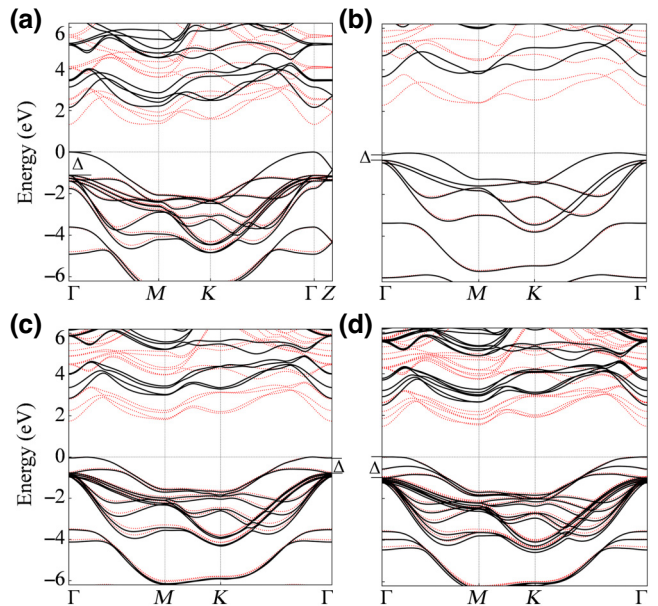


FIG. 2. The  $GW$  quasiparticle (black solid) and density-functional theory Perdew-Burke-Ernzerhof (red dotted) band structures of (a) bulk, (b) monolayer, (c) bilayer, and (d) trilayer GaSe. The VBMs are shifted to zero in the plots.  $\Delta$  is the energy splitting of the top valence bands (derived from  $p_z$  and  $p_x + p_y$ ) at  $\Gamma$ .

It is instructive to compare the band structures of the bulk and monolayer systems [Figs. 2(a) and 2(b)]. The interlayer interaction, although considered weak (with an interlayer binding energy of about 19 meV/atom), results in a surprisingly large splitting of the band-edge states and significant changes in band dispersions of the bulk phase compared with that of the monolayer. The valence band splitting  $\Delta$  (defined in Fig. 2) increases from 0.25 eV (monolayer) to 1.13 eV (bulk).

One interesting observation is the dispersion of the top valence band of monolayer GaSe: the VBM is shifted away (by  $\Delta k$ ) from  $\Gamma$ , resulting in a slightly indirect band gap and a MH-like band dispersion near the VBM (also shown schematically in Fig. 3). The bulk structure, on the other hand, has a VBM at  $\Gamma$ . The calculated parameters  $\Delta k$  and  $\Delta E$  [defined in Fig. 3(a)] for few-layer systems are listed in Table II. Both  $\Delta E$  and  $\Delta k$  decrease quickly as the number of layers increases, and for the bulk system, a direct gap at the  $\Gamma$  point is formed. The MH-like dispersion also gives an extraordinary sharp density of states (DOS) near the VBM for the monolayer system, as shown in Fig. 3(c). The decomposition of the DOS indicates that the top valence band predominantly has the Se- $p_z$  character.

The interlayer  $p_z$ - $p_z$  coupling greatly suppresses this MH-like dispersion and the DOS near the VBM as the number of layers increases. These interesting features have been discussed in great detail previously [10]. The Se- $p_x + p_y$  component [colored blue in Figs. 3(b) and 3(c)],

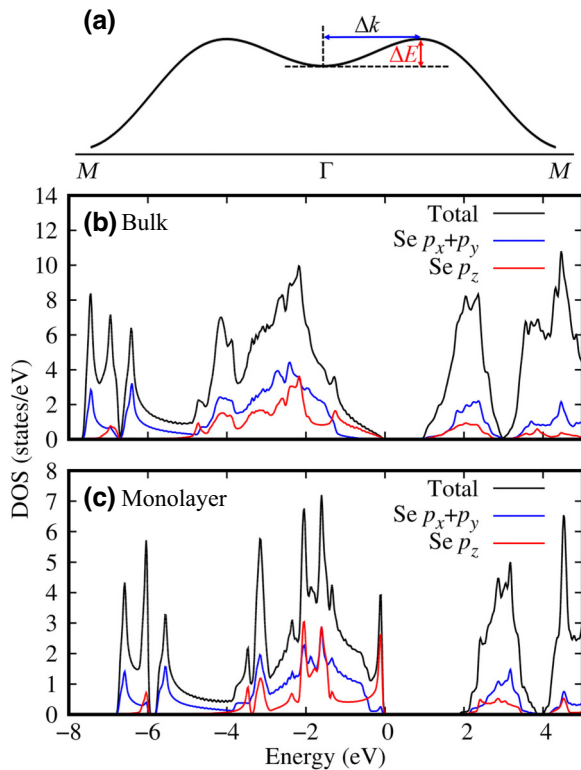


FIG. 3. Schematic of the Mexican-hat-like dispersion of few-layer GaSe around the  $\Gamma$  point (a) and the density of states (DOS) of the bulk (b) and monolayer (c) GaSe.

on the other hand, is minimally affected by the interlayer coupling. The large  $\Delta E$  and  $\Delta k$  for the monolayer and their layer dependence explain the significant decrease in PL emission intensity with a decreasing number of layers and the disappearance of PL signals in monolayer

TABLE II. Parameters  $\Delta E$  (meV) and  $\Delta k$  ( $\text{\AA}^{-1}$ ) [defined in Fig. 3(a)] for the MH-like dispersion of the top valence band of few-layer GaSe.

	Monolayer	Bilayer	Trilayer
$\Delta E$	128	47	18
$\Delta k$	0.17	0.11	0.06

GaSe [14]. PL from the bilayer and trilayer systems (although much weaker compared with that from bulk GaSe) is likely due to thermal population of the excited carriers, since the direct-indirect energy difference  $\Delta E$  is comparable with or smaller than the thermal energy at room temperature. Other mechanisms that may contribute to the PL in the bilayer and trilayer GaSe include phonon-assisted PL [40,41] and exciton dispersion effects [42].

Table III compares the calculated (DFT and  $GW$ ) band gap with those measured by various methods. For few-layer systems, we list both the direct gap at the  $\Gamma$  point and the minimum gap, calculated with DFT and  $GW$  methods. The calculated minimum quasiparticle band gaps ( $E_{g,\min}^{GW}$  in Table III, highlighted in bold) of few-layer systems agree reasonably well (<0.2 eV) with those measured by STS [ $E_g^{\text{QP}}(\text{exp})$  in Table III, highlighted in bold] [16]. Band gaps measured by optical techniques (e.g., CL or PL) [ $E_g^{\text{opt}}(\text{exp})$  in Table III, highlighted in bold] should be compared with the excitonic gaps ( $E_g^{\text{ex}}$  in Table III, to be discussed later), more specifically, the calculated bright excitonic gap highlighted in bold. For example, the calculated minimum excitonic gap of monolayer GaSe is 3.09 eV. However, this value cannot be compared directly with experimentally measured optical gaps since the first exciton is a dark exciton. The calculated bright excitonic gap for monolayer GaSe is 3.39 eV, which compares well

TABLE III. Quasiparticle and optical band gaps (in eV) of few-layer and bulk GaSe: Comparison between theory and experiment.  $\Delta$  is the  $GW$ -predicted valence band splitting (in eV) at  $\Gamma$ , as defined in Fig. 3.

	Monolayer	Bilayer	Trilayer	Bulk
$E_{g,\Gamma}^{\text{PBE}}$	2.26	1.65	1.36	1.17
$E_{g,\min}^{\text{PBE}}$	2.13	1.60	1.34	1.17
$E_{g,\Gamma}^{GW}$	3.77	2.89	2.49	2.14
$E_{g,\min}^{GW}$	<b>3.64</b>	<b>2.84</b>	<b>2.47</b>	<b>2.14</b>
$E_g^{\text{QP}}(\text{exp})$	<b>3.5<sup>a</sup></b>	<b>3.00<sup>a</sup></b>	<b>2.30<sup>a</sup></b>	<b>2.13<sup>b</sup></b>
$E_g^{\text{ex}}$	3.09 (dark) <b>3.39 (bright)</b>	<b>2.49 (weak)</b>	2.20 (dark) <b>2.32 (weak)</b>	<b>2.10 (bright)</b>
$E_g^{\text{opt}}(\text{exp})$	<b>3.3<sup>c</sup></b>	<b>2.44<sup>d</sup></b>	<b>2.28<sup>d</sup></b>	<b>1.99<sup>d</sup>, 2.11<sup>e</sup></b>
$\Delta$	0.25	0.74	1.02	1.13

<sup>a</sup>STS [16];

<sup>b</sup>Optical absorption [43,44];

<sup>c</sup>CL [15];

<sup>d</sup>PL peak positions [14];

<sup>e</sup>Optical absorption [43–45]

with the experimental result of 3.3 eV. For the bilayer system, the first exciton state is bright (albeit weak). For bulk GaSe, since the exciton binding energy is small, the measured optical gap agrees well with the calculated  $GW$  gap.

We mention that  $GW$  results calculated using different GPP models (or without the use of GPP models) can sometimes differ significantly. In particular, it has been shown that the HL GPP model often gives larger band gaps compared with other models [46,47]. However, the accuracy of  $GW$  calculations is a fairly complex issue. In addition to various approximations made in the calculations, numerical convergence is also an important issue [23,25,26,48,49]. Detailed discussion of these issues is beyond the scope of this work. In the next two sections, we discuss the excitonic structure and optical properties in more detail.

### C. Excitonic structure and optical properties of bulk GaSe

Several experiments have been conducted to study the optical properties of bulk [43–45,50,51] and few-layer [14,15,43–45,50–52] GaSe. However, optical property calculations have only been reported for monolayer GaSe [36,53,54], and there is a lack of systematic studies of layer-dependent excitonic structure and optical properties of these systems. In this work, the excitonic structure and optical properties of few-layer and bulk GaSe are investigated by solving the BSE [18], which is reduced to an eigenvalue problem within the Tamm-Dancoff approximation,

$$(E_{c\mathbf{k}} - E_{v\mathbf{k}})A_{vc\mathbf{k}}^S + \sum_{v'c'\mathbf{k}'} \langle v\mathbf{c}\mathbf{k} | K^{eh} | v'c'\mathbf{k}' \rangle A_{v'c'\mathbf{k}'}^S = \Omega^S A_{vc\mathbf{k}}^S, \quad (1)$$

where  $E_{c\mathbf{k}}$  and  $E_{v\mathbf{k}}$  are the quasiparticle energies of the conduction and valence states;  $A_{vc\mathbf{k}}^S$  is the eigenvector (i.e., the  $e$ - $h$  amplitude) that defines the exciton wave function,

$$\Psi^S(\mathbf{r}_e, \mathbf{r}_h) = \sum_{vc\mathbf{k}} A_{vc\mathbf{k}}^S \psi_{c\mathbf{k}}(\mathbf{r}_e) \psi_{v\mathbf{k}}^*(\mathbf{r}_h), \quad (2)$$

and  $K^{eh}$  is the  $e$ - $h$  interaction kernel. Solving the above eigenvalue problem gives the  $e$ - $h$  excitation energy  $\Omega^S$ , and the wave function of the excitonic state  $|S\rangle$ . The imaginary part of the macroscopic transverse dielectric function

$$\epsilon_2(\omega) = \frac{16\pi^2 e^2}{\omega^2} \sum_S |\vec{\mathbf{e}} \cdot \langle 0 | \vec{v} | S \rangle|^2 \delta(\omega - \Omega^S), \quad (3)$$

where  $\vec{v}$  is the velocity operator,  $\vec{\mathbf{e}}$  is the polarization vector of the light,  $\omega$  is the energy of the photon.

Bulk GaSe is known to have a highly anisotropic optical response [43–45,50,51]: strong excitonic absorption is observed near the band gap (2.11 eV at low temperatures) for a photon polarization ( $\mathbf{E}$ ) direction parallel to the  $c$  axis ( $\mathbf{E} \parallel c$ ); for  $\mathbf{E}$  parallel to the  $a$ - $b$  plane ( $\mathbf{E} \parallel a-b$ ), however, no significant optical activities are observed below 3.0 eV. Our theoretical findings, as presented in Fig. 4, are consistent with the experiment. In particular, the calculated first excitonic absorption peak for  $\mathbf{E} \parallel c$  at 2.10 eV (upper panel of Fig. 4) agrees very well with the low-temperature experimental results of about 2.11 eV [43–45]. In the upper panel of Fig. 4, we also show the energies of excitonic states as vertical lines scaled by the dipole transition matrix elements for polarization  $\mathbf{E} \parallel c$ . The strong absorption peak for  $\mathbf{E} \parallel a-b$  at about 3.70 eV (lower panel of Fig. 4) also agrees well with the experimental value of 3.63 eV [50].

In addition to the optical absorption shown in Fig. 4, understanding the strength of the  $e$ - $h$  interaction and the exciton binding energies ( $E_b^{\text{ex}}$ ) of the excitons is also of great interest. The exciton binding energy is often loosely defined as the difference between the quasiparticle excitation gap and the excitonic gap, i.e.,  $E_b^{\text{ex},S} = E_g^S - \Omega^S$ . The quasiparticle gap  $E_g^S$ , however, must be understood as the weighted average of the noninteracting  $e$ - $h$  excitation gap

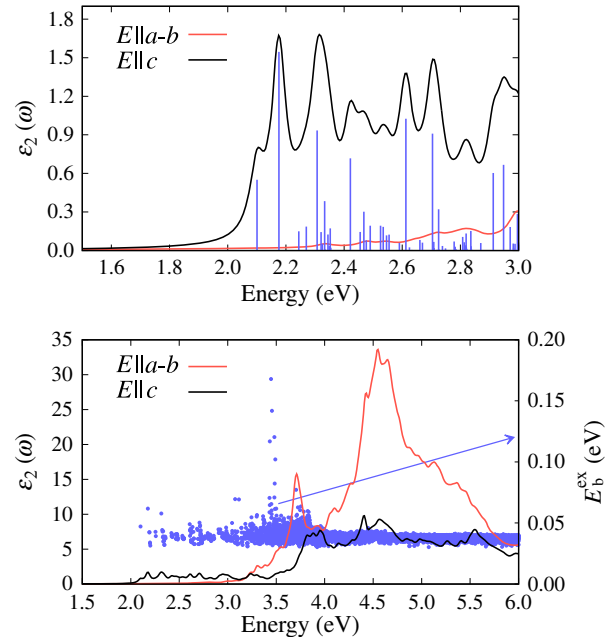


FIG. 4. Polarization-dependent imaginary part of the dielectric function of bulk GaSe. The vertical lines in the upper panel show the position of excitonic states scaled by their dipole transition matrix elements in Eq. (3) for polarization  $\mathbf{E} \parallel c$ . The lower panel shows the dielectric function over an extended energy range. The binding energies (right y axis) of the excitons are shown as blue dots in the lower panel.

[55,56], defined as follows for any excitonic state  $|S\rangle$ :

$$E_g^S = \sum_{vck} |A_{vck}^S|^2 (E_{ck} - E_{vk}). \quad (4)$$

In the bottom panel of Fig. 4, we show the calculated binding energies (blue dots in the figure) for all excitonic states below 6 eV for bulk GaSe. Most states have a binding energy smaller than 50 meV. However, a few excitonic states that are well above the fundamental band gap (at about 3.49 eV) have surprisingly large binding energies, with one state having a binding energy as large as 168 meV. The dramatic variation of the exciton binding energy from state to state and the abnormally large binding energies for some exciton states in such a moderate-gap bulk semiconductor deserve scrutiny. Although the binding energy of an excitonic state is generally related to the spread (or localization) of the exciton wave function, it is not yet well understood why some states are more localized than others in a single system.

To this end, we investigate the distribution (spread) of the exciton wave functions in both momentum and real spaces. First, we define the band- and  $k$ -resolved hole and electron amplitudes,

$$|A_{vk}^S|^2 = \sum_c |A_{vc\bar{k}}^S|^2, \quad (5)$$

$$|A_{ck}^S|^2 = \sum_v |A_{vck}^S|^2, \quad (6)$$

and the  $k$ -resolved pair amplitude,

$$|A_{\bar{k}}^S|^2 = \sum_{vc} |A_{vc\bar{k}}^S|^2. \quad (7)$$

These functions reveal the distribution of the hole, electron, and the  $e-h$  pair in the  $k$  space of a given state  $|S\rangle$ . The top panels of Fig. 5 show  $|A_{vk}^S|^2$  and  $|A_{ck}^S|^2$  of two representative excitonic states,  $A$  and  $B$ . Whereas exciton  $A$  (top left panel) has a calculated binding energy of about 47 meV, that of exciton  $B$  (top right panel) is 168 meV. The electron and hole amplitudes of exciton  $A$  are highly concentrated in a small region of the BZ (in this case, near the  $\Gamma$  point). In contrast, for exciton  $B$ , these amplitudes are rather delocalized in the momentum space over which there is a pair of valence and conduction bands that are nearly parallel in a portion of the BZ. It is these (nearly) parallel valence and conduction bands that offer a large number of  $e-h$  pairs across the BZ with similar excitation energies, giving rise to excitonic states that are delocalized in momentum space.

The localization (or delocalization) of the electron and hole amplitudes in momentum space is highly correlated with the spread of the exciton wave function in real space. In the bottom two panels of Fig. 5, we plot the isosurface of the square of the electron part of the exciton wave function

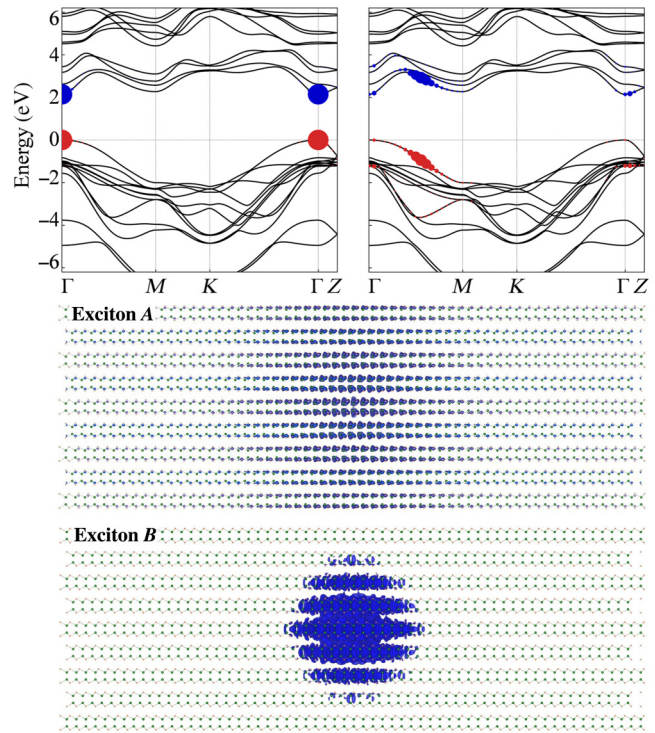


FIG. 5. The band- and  $k$ -resolved electron and hole amplitudes of the first exciton (exciton  $A$ , top left panel,  $\Omega^S = 2.10$  eV) and the exciton with the largest binding energy (exciton  $B$ , top right panel,  $\Omega^S = 3.45$  eV) of bulk GaSe. The lower panels are the real-space distribution of electron charge density of the two excitons. The hole position is fixed at the center of the supercell.

[defined as  $\rho_e(\mathbf{r}_e; \mathbf{r}_h) = |\Psi^S(\mathbf{r}_e, \mathbf{r}_h)|^2 / \int |\Psi^S(\mathbf{r}_e, \mathbf{r}_h)|^2 d\mathbf{r}_e$ ] by fixing the hole position  $\mathbf{r}_h$  near the center of the cell. For exciton  $A$ , the electron wave function is rather delocalized. This is in sharp contrast with that of exciton  $B$ , for which the electron wave function is highly localized near the hole. The existence of such strongly localized (strongly bound, thus potentially long-lifetime) excitons in the excitation continuum might have interesting implications in the dynamics of excitons and deserves further investigations. We would like to mention that the distribution of the electron density does not depend sensitively on the choice of the hole position; see the Supplemental Material at [29] Fig. S3 for the plots of the electron density distribution with different choices of hole position.

To gain a more quantitative understanding, we define a measure for the spread of the electron,  $r_e = \langle \mathbf{r}_e^2 \rangle^{-1/2}$ , for a given excitonic state  $|S\rangle$  and a fixed hole position  $\mathbf{r}_h$ ,

$$\langle \mathbf{r}_e^2 \rangle = \int |\Psi^S(\mathbf{r}_e, \mathbf{r}_h)|^2 (\mathbf{r}_e - \mathbf{r}_h)^2 d\mathbf{r}_e / \int |\Psi^S(\mathbf{r}_e, \mathbf{r}_h)|^2 d\mathbf{r}_e. \quad (8)$$

We expect that the exciton binding energy would be inversely proportional to the size of the exciton in real

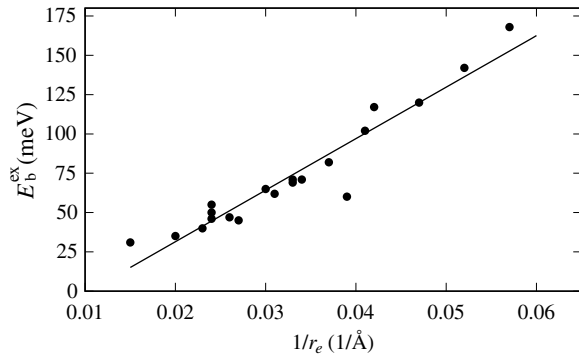


FIG. 6. Calculated exciton binding energy vs  $1/r_e$  for 20 excitons, showing a nearly linear relationship between the exciton binding energy and the inverse of the size of exciton.

space. Indeed, our calculations of about 20 excitons suggest a nearly linear relationship between the exciton binding energy and  $1/r_e$  as shown in Fig. 6. It should be mentioned that the above definition of the electron radius may appear rather arbitrary since it depends on the choice of the hole position  $\mathbf{r}_h$ . However, this is not the case. In fact, the electron radius defined this way is independent of the choice of the hole position (within numerical errors); see Table S1 in the Supplemental Material at [29] for the effective electron radius of the exciton of bulk GaSe with the largest binding energy calculated with different choices of hole position.

It should be mentioned that it is extremely difficult to carry out fully converged BSE calculations for the excitonic properties, especially the binding energies, of delocalized excitons. The measured binding energy of the lowest excitonic state in bulk GaSe ranges from 20 to 22 meV [43,44,51], to be compared with the theoretical value of 47 meV calculated using a  $36 \times 36 \times 8$   $k$  grid, although such a  $k$ -grid density is sufficient to converge the overall features of the optical absorption spectra shown in Fig. 4. Additional details can be found in Fig. S2 of the Supplemental Material at [29]. The calculated binding energies of most excitonic states (except for the localized states discussed previously) are hardly converged with respect to the  $k$ -grid density. Unfortunately, exciton calculations using  $k$ -grid densities higher than  $36 \times 36 \times 8$  for this system are beyond our local computing capacity. In fact, even with a  $36 \times 36 \times 8$   $k$  grid, the  $e$ - $h$  Hamiltonian matrix size is already about  $500\,000 \times 500\,000$  in this case.

Figure 7 shows the convergence behavior of the binding energy of the first exciton and the averaged binding energy of all excitonic states below 6.0 eV. It is interesting to note that the binding energies scale approximately linearly with  $\sqrt{1/N_k}$ , where  $N_k = N_x \times N_y \times N_z$  is the total number of  $k$  points used in expanding the exciton wave functions [see Eq. (1)]. Since the volume over which the exciton wave functions are represented is  $V = N_k \times V_{\text{cell}}$ ,

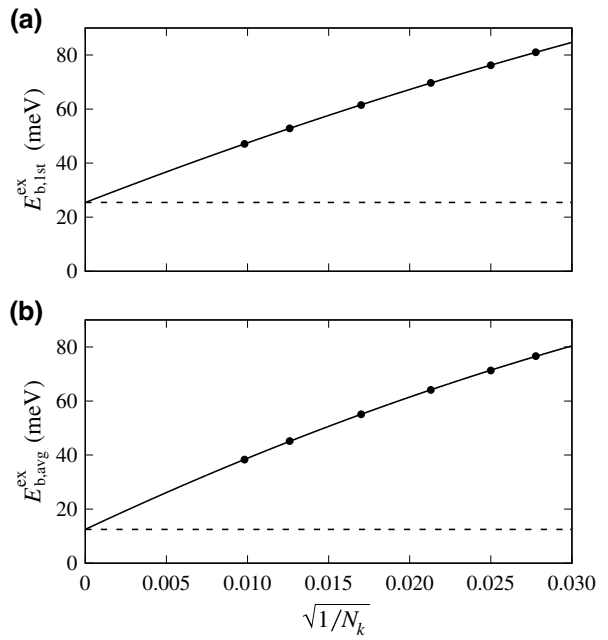


FIG. 7. Binding energy of the first excitonic state (a) and the averaged binding energy of all excitons below 6 eV (b) of bulk GaSe as a function of  $\sqrt{1/N_k}$  ( $N_k = N_x \times N_y \times N_z$  is number of  $k$  points used in the calculations). The coarsest  $k$  grid is  $18 \times 18 \times 4$  and the finest is  $36 \times 36 \times 8$ . Solid dots are the calculated values and solid curves are the fitted results. Dashed lines show the extrapolation of the binding energy to an infinitely dense  $k$  grid, giving a binding energy of 25.4 meV for the first exciton, and 12.5 meV for all excitons below 6 eV.

an enormously large cell (i.e., a very high  $k$ -grid density) is needed to converge the properties of delocalized excitons in bulk semiconductors. The extrapolated exciton binding energy to an infinitely dense  $k$  grid is 25.4 meV for the first exciton, which agrees well with the experimental value of 20–22 meV [43,44,51].

#### D. Layer-dependent excitonic structure and optical properties

Next, we investigate the effects of layer thickness on the excitonic structure and optical properties of GaSe. It is instructive to compare  $\varepsilon_{00}^{-1}(q)$  (the  $q$ -dependent head element of the inverse dielectric matrix) of monolayer, multilayer, and bulk systems, as shown in Fig. 8, where  $q$  is along the  $a$ - $b$  plane. The rapid upshift of this function at small  $q$  (approaching 1 as  $q$  approaches 0) is characteristic of 2D materials. This behavior also explains the extremely slow convergence of the calculated quasiparticle properties with respect to the BZ sampling  $k$ -grid density unless special sampling techniques [26,57,58] are used. With the increasing layer thickness, the dielectric screening [ $1/\varepsilon_{00}^{-1}(q)$ ] gradually increases. However, even for the trilayer system (the thickness of trilayer GaSe is about

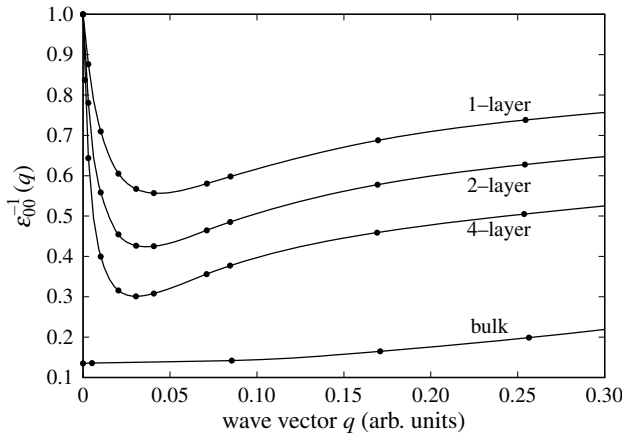


FIG. 8. Layer-thickness dependence of the head element of the inverse dielectric matrix  $\epsilon_{00}^{-1}(q)$  ( $q$  is in units of  $2\pi/a$ ), showing the evolution of the dielectric screening effects from monolayer to bulk systems.

21 Å), the dielectric screening is still significantly reduced compared with that of the bulk material.

The layer-thickness-dependent dielectric screening and the interlayer coupling will significantly affect the excitonic structure and optical absorption of these systems. Figure 9 compares the calculated optical absorption spectra (for  $E \parallel a-b$ , black curves) and excitonic structure (exciton binding energy versus exciton energy, shown in blue dots) of few-layer and bulk GaSe. The vertical black dashed line indicates the direct quasiparticle gap  $E_g$  at  $\Gamma$ ; the shaded areas around  $E_g$  highlight the low-energy excitonic states of each system, which are then expanded in the narrow horizontal boxes atop each main plot to show their optical activities. Each vertical line in the narrow horizontal boxes indicates an excitonic state, color-coded according to its optical dipole matrix element. Note that for 2D materials, the absolute value of the calculated  $\varepsilon_2$  bears no significance since it depends on the volume of the calculation unit cell (more precisely, the  $c$  lattice constant). However, the main features of the absorption spectra can be directly compared with the experiment.

Low-energy excitonic states and optical properties are highly layer-thickness dependent, and the systematic changes in the first two excitonic absorption peaks can be clearly seen as the layer thickness increases. Although all few-layer systems have a large number of below-the-gap (BTG) excitonic states, the number of these BTG excitons decreases significantly with increasing layer thickness as a result of reduced  $e-h$  interaction. For bulk GaSe, we observe only one excitonic state below the fundamental gap. It is possible that one needs higher density  $k$  grids to resolve more excitonic Rydberg states below the band gap. Another interesting observation is that only the monolayer shows strong optical absorption below the band gap.

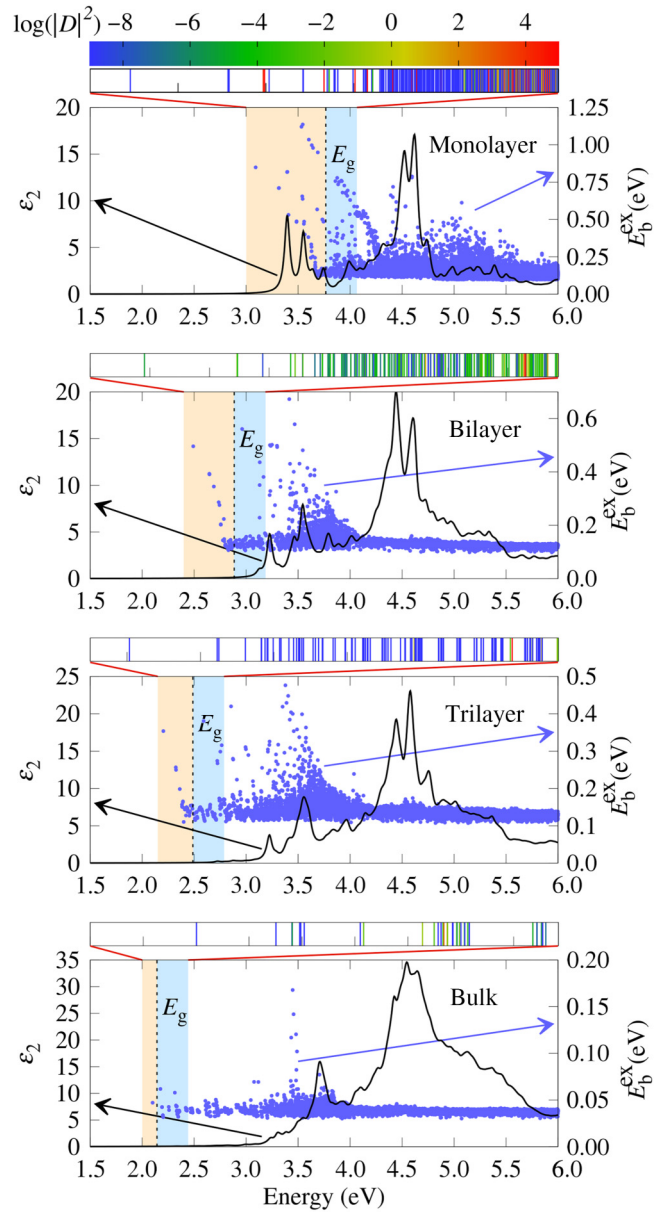
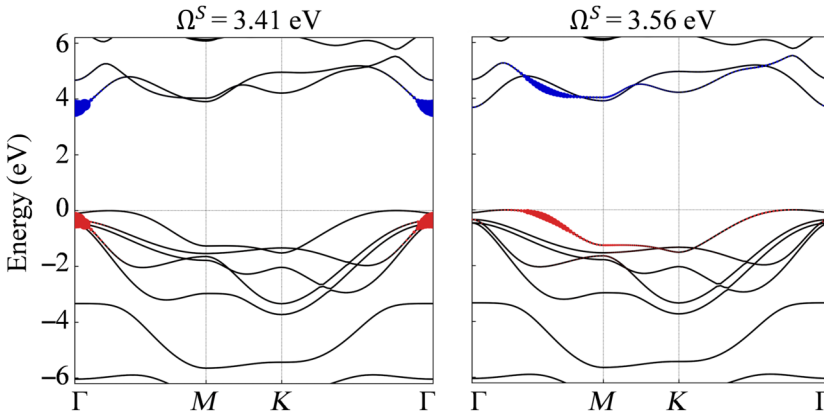


FIG. 9. Optical absorption spectra ( $E \parallel a-b$ , black curves) and exciton binding energies  $E_b^{\text{ex}}$  (blue dots) of few-layer and bulk GaSe. The vertical black dashed line is the position of the quasi-particle band gap ( $E_g$ ) at  $\Gamma$ . An energy broadening of 0.03 eV is used in the calculation of  $\varepsilon_2$ . The shaded areas highlight the excitonic states slightly below (light orange area) and above (light blue) the fundamental gap. The low-energy excitonic states within the shaded area, color-coded with their dipole matrix elements, are shown in the extended horizontal boxes on top of the main plots.

The first absorption peak is very strong for monolayer GaSe, whereas in the few-layer and bulk systems, it is the second peak that is more pronounced. For the monolayer system, the first absorption peak can be attributed to a pair of excitons formed by the Se  $p_x + p_y$ -derived hole states (colored red in the left panel of Fig. 10) and primarily Ga



*s*-derived electron states (colored blue in the left panel of Fig. 10) near the  $\Gamma$  point, whereas the second absorption peak is associated with a single exciton mainly composed of  $p_z$ -derived nearly parallel valence and conduction bands midway along the  $\Gamma$  to  $M$  path. These features are similar to those shown in Fig. 5 in the case of bulk GaSe. See Fig. S4 in the Supplemental Material at [29] for plots of the  $e$ - $h$  pair amplitudes [Eq. (7)] of a few selected excitonic states.

Another interesting observation of the plot of exciton binding energy versus excitation energy is that, on top of the seemingly random distribution of the exciton binding energy, the binding energies of some states seem to group into a narrow shell-like distribution. These structures arise from the presence of nearly parallel valence and conduction bands, as we have discussed in great detail in our recent works [55,56].

While the changes in the overall absorption spectra from the monolayer to bilayer are highly significant (suggesting the strong effects from the enhanced screening and interlayer coupling), those from bilayer GaSe to bulk are relatively minor. This is somewhat surprising considering that the excitonic structure (positions and distribution of the excitons, their binding energies, etc.) are very different in these systems (i.e., bilayer, trilayer, and bulk) as can be seen from Fig. 9. The strong absorption peak around 4.5 eV is fairly robust across all systems, indicating that optical absorption near this energy is dominated by intralayer excitons.

The calculated exciton binding energies decrease systematically with increasing layer thickness. For bulk GaSe, most excitonic states have binding energies smaller than 50 meV, with a few states having noticeably large binding energy states around 3.5 eV, as discussed in Sec. III C. Table IV shows the minimum quasiparticle band gaps, excitation energies, and binding energies of the first exciton and the exciton with the largest binding energy of few-layer and bulk GaSe. We also show the binding energy of the first exciton using the conventional definition, i.e.,  $E_{g,\min}^{GW} - \Omega^1$ , in parentheses for comparison. We would like to point out that this definition is only valid for the excitons

FIG. 10. The band- and  $k$ -resolved electron and hole amplitudes of first bright exciton with an excitation energy  $\Omega^S = 3.41$  eV (the first absorption peak, left panel) and second bright exciton with  $\Omega^S = 3.56$  eV (the second absorption peak, left panel) of monolayer GaSe.

for which the electron and hole states are derived from QP states that define the fundamental band gap, which is often not the case.

The excitonic gap decreases monotonically with the increasing layer thickness. The binding energy decreases by over 350 meV (or more than 40%) going from the monolayer to the bilayer system. Interestingly, the excitonic gap of the trilayer is already very close to that of the bulk. However, the binding energy of the first exciton of trilayer GaSe is still more than 10 times larger than that of bulk GaSe. The largest binding energy increases from 168 meV (bulk) to 1.14 eV (monolayer), as shown in Table IV. We mention that the excitonic gap (i.e., the energy of the first exciton) may or may not correspond to the measured optical gap depending on the optical dipole matrix element of the transition. For example, the first exciton is dark for the few-layer systems. The calculated layer-dependent optical gaps, as measured by the first bright exciton energies, agree very well with the experiment (see Table III).

Finally, it should be mentioned that for 2D materials,  $\varepsilon_2$  depends on the thickness of the vacuum layer included in the calculations. Therefore, the absolute values of  $\varepsilon_2$

TABLE IV. Quasiparticle band gaps and exciton energies of few-layer and bulk GaSe. Only the first exciton and the exciton with the largest binding energy are shown. The exciton binding energies are calculated using the quasiparticle gap defined in Eq. (4). Exciton binding energies calculated using the conventional definition (i.e.,  $E_{g,\min}^{GW} - \Omega^1$ ) are shown in parentheses. The  $E_b^1$  for bulk GaSe is obtained by extrapolating theoretical results to an infinitely dense  $k$  grid.

	Monolayer	Bilayer	Trilayer	Bulk
$E_{g,\min}^{GW}$	3.64	2.84	2.47	2.14
$\Omega^1$ (eV)	3.09	2.49	2.20	2.10
$E_b^1$ (meV)	849 (550)	493 (350)	354 (270)	25 (25)
$\Omega^{\max}$ (eV)	3.54	3.42	3.38	3.45
$E_b^{\max}$ (meV)	1136	673	476	168

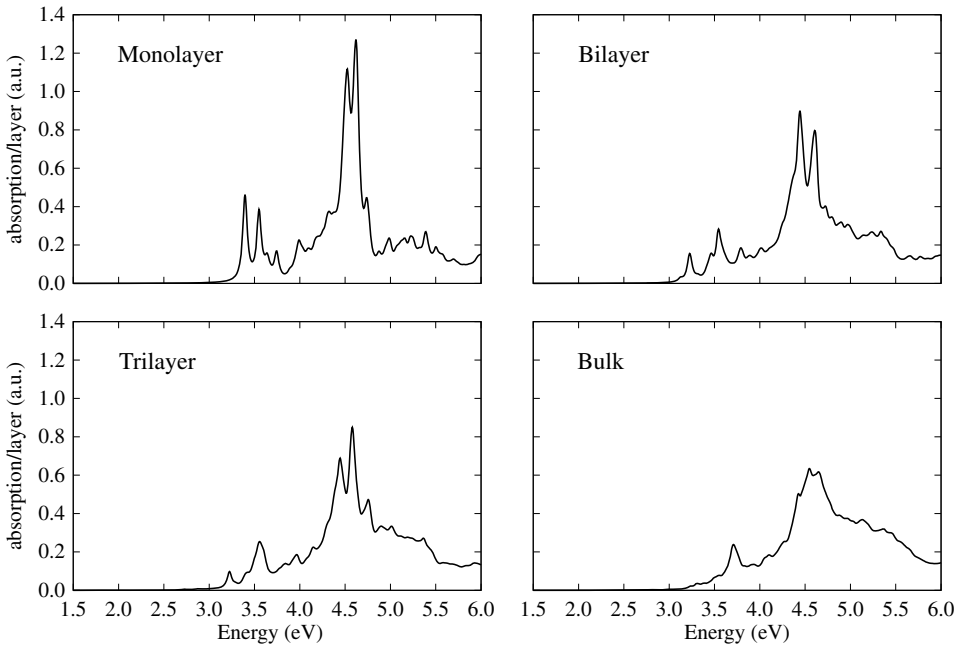


FIG. 11. Evolution of layer-thickness normalized absorbance (in atomic units) of few-layer and bulk GaSe.

for 2D materials bear no significance and cannot be compared directly with that of bulk. However, the evolution of the excitonic properties (i.e., the position and relative strength of the excitonic absorption peaks, and the exciton binding energies) shown in Fig. 9 can be compared directly with experiment. To gain better understanding of the evolution of the optical absorption, we show in Fig. 11 layer-normalized absorbance [59], defined as  $A(\omega) = L(\omega/c)\epsilon_2(\omega)/N$ , where  $L$  is the lattice constant along the  $c$  axis, and  $N$  is the number of layers (1 for monolayer GaSe, 2 for bilayer, 3 for trilayer, and 2 for bulk). This quantity better shows the evolution of the absorption efficiency with layer thickness. Overall, the monolayer shows highest absorption efficiency (per layer).

#### IV. SUMMARY

We have performed detailed  $GW$  plus BSE calculations for few-layer and bulk GaSe. The unique excitonic structures and exciton binding energies of these systems are carefully analyzed to illustrate the effects of interlayer coupling and layer-thickness-dependent dielectric screening on excited-state properties of GaSe. Our results also help resolve apparent discrepancies between different experiments. The interlayer coupling greatly suppresses the Mexican-hat-like dispersion of the top valence band, explaining the greatly enhanced PL as layer thickness increases. We find the delocalization (localization) of excitonic wave functions in the BZ results in their localization (delocalization) in real space and increased (decreased) exciton binding energies. The exciton binding energy is inversely proportional to the spread of the averaged  $e\text{-}h$

separation (i.e., spread of the exciton wave function). The presence of (nearly) parallel valence and conduction bands greatly facilitates the delocalization of exciton wave functions in the BZ, leading to strongly localized wave functions in real space, and thus greatly enhanced exciton binding energy. The calculated maximum exciton binding energy decreases from 1.14 eV (monolayer) to 0.17 eV (bulk). For delocalized excitons, an extremely dense  $k$  grid may be needed to converge the calculated exciton binding energy. The calculated exciton binding energy of the lowest excitonic state of bulk GaSe, after extrapolating to the converged value, agrees very well with experimental result. The changes in the overall absorption spectra from the monolayer to the bilayer are highly significant, and the monolayer is the only case that exhibits bright exciton absorption (for polarization  $\mathbf{E}||a\text{-}b$ ) below the fundamental gap.

#### ACKNOWLEDGMENTS

Work at HDU and SHU was supported by the National Natural Science Foundation of China (Grants No. 11929401, No. 12074241, No. 52130204) and Key Research Project of Zhejiang Lab (Grant No. 2021PE0AC02). W.G. was supported by National Natural Science Foundation of China (Grant No. 12104080). Work at UB was supported by the National Science Foundation under Grant No. DMREF-1626967. We acknowledge computational support from the Center for Computational Research, University at Buffalo, SUNY.

- [1] M. Long, P. Wang, H. Fang, and W. Hu, Progress, challenges, and opportunities for 2D material based photodetectors, *Adv. Funct. Mater.* **29**, 1803807 (2019).
- [2] H. Cai, Y. Gu, Y.-C. Lin, Y. Yu, D. B. Geohegan, and K. Xiao, Synthesis and emerging properties of 2D layered III–VI metal chalcogenides, *Appl. Phys. Rev.* **6**, 041312 (2019).
- [3] D. A. Bandurin, A. V. Tyurnina, G. L. Yu, A. Mishchenko, V. Zólyomi, S. V. Morozov, R. K. Kumar, R. V. Gorbachev, Z. R. Kudrynskyi, and S. Pezzini, High electron mobility, quantum Hall effect and anomalous optical response in atomically thin InSe, *Nat. Nanotechnol.* **12**, 223 (2017).
- [4] S. R. Tamalampudi, Y.-Y. Lu, U. Rajesh Kumar, R. Sankar, C.-D. Liao, C.-H. Cheng, F. C. Chou, and Y.-T. Chen, High performance and bendable few-layered InSe photodetectors with broad spectral response, *Nano Lett.* **14**, 2800 (2014).
- [5] X. Li, M.-W. Lin, A. A. Puretzky, J. C. Idrobo, C. Ma, M. Chi, M. Yoon, C. M. Rouleau, I. I. Kravchenko, and D. B. Geohegan, Controlled vapor phase growth of single crystalline, two-dimensional GaSe crystals with high photoresponse, *Sci. Rep.* **4**, 5497 (2014).
- [6] M. Isik, E. Tugay, and N. Gasanly, Temperature-dependent optical properties of GaSe layered single crystals, *Philos. Mag.* **96**, 2564 (2016).
- [7] C. Wei, X. Chen, D. Li, H. Su, H. He, and J.-F. Dai, Bound exciton and free exciton states in GaSe thin slab, *Sci. Rep.* **6**, 33890 (2016).
- [8] H. Kamimura and K. Nakao, Band structures and optical properties of semiconducting layer compounds GaS and GaSe, *J. Phys. Soc. Jpn.* **24**, 1313 (1968).
- [9] T. Cao, Z. Li, and S. G. Louie, Tunable magnetism and half-metallicity in hole-doped monolayer GaSe, *Phys. Rev. Lett.* **114**, 236602 (2015).
- [10] D. V. Rybkovskiy, A. V. Osadchy, and E. D. Obraztsova, Transition from parabolic to ring-shaped valence band maximum in few-layer GaS, GaSe, and InSe, *Phys. Rev. B* **90**, 235302 (2014).
- [11] D. A. Bandurin, A. V. Tyurnina, L. Y. Geliang, A. Mishchenko, V. Zólyomi, S. V. Morozov, R. K. Kumar, R. V. Gorbachev, Z. R. Kudrynskyi, and S. Pezzini, High electron mobility, quantum Hall effect and anomalous optical response in atomically thin InSe, *Nat. Nanotechnol.* **12**, 223 (2017).
- [12] O. Del Pozo-Zamudio, S. Schwarz, M. Sich, I. Akimov, M. Bayer, R. Schofield, E. Chekhovich, B. Robinson, N. Kay, and O. Kolosov, Photoluminescence of two-dimensional GaTe and GaSe films, *2D Mater.* **2**, 035010 (2015).
- [13] D. Andres-Penares, A. Cros, J. P. Martínez-Pastor, and J. F. Sánchez-Royo, Quantum size confinement in gallium selenide nanosheets: Band gap tunability versus stability limitation, *Nanotechnology* **28**, 175701 (2017).
- [14] D. J. Terry, V. Zólyomi, M. Hamer, A. V. Tyurnina, D. G. Hopkinson, A. M. Rakowski, S. J. Magorrian, N. Clark, Y. M. Andreev, and O. Kazakova, Infrared-to-violet tunable optical activity in atomic films of GaSe, InSe, and their heterostructures, *2D Mater.* **5**, 041009 (2018).
- [15] C. S. Jung, F. Shojaei, K. Park, J. Y. Oh, H. S. Im, D. M. Jang, J. Park, and H. S. Kang, Red-to-ultraviolet emission tuning of two-dimensional gallium sulfide/selenide, *ACS Nano* **9**, 9585 (2015).
- [16] Z. B. Aziza, D. Pierucci, H. Henck, M. G. Silly, C. David, M. Yoon, F. Sirotti, K. Xiao, M. Eddrief, and J.-C. Girard, Tunable quasiparticle band gap in few-layer GaSe/graphene van der Waals heterostructures, *Phys. Rev. B* **96**, 035407 (2017).
- [17] M. S. Hybertsen and S. G. Louie, Electron correlation in semiconductors and insulators: Band gaps and quasiparticle energies, *Phys. Rev. B* **34**, 5390 (1986).
- [18] M. Rohlfing and S. G. Louie, Electron-hole excitations and optical spectra from first principles, *Phys. Rev. B* **62**, 4927 (2000).
- [19] H. Peng, Z.-H. Yang, J. P. Perdew, and J. Sun, Versatile van der Waals density functional based on a meta-generalized gradient approximation, *Phys. Rev. X* **6**, 041005 (2016).
- [20] G. Kresse and J. Furthmüller, Efficient iterative schemes for *ab initio* total-energy calculations using a plane-wave basis set, *Phys. Rev. B* **54**, 11169 (1996).
- [21] S. Ismail-Beigi, Truncation of periodic image interactions for confined systems, *Phys. Rev. B* **73**, 233103 (2006).
- [22] J. Deslippe, G. Samsonidze, D. A. Strubbe, M. Jain, M. L. Cohen, and S. G. Louie, BerkeleyGW: A massively parallel computer package for the calculation of the quasiparticle and optical properties of materials and nanostructures, *Comput. Phys. Commun.* **183**, 1269 (2012).
- [23] W. Gao, W. Xia, X. Gao, and P. Zhang, Speeding up GW calculations to meet the challenge of large scale quasiparticle predictions, *Sci. Rep.* **6**, 36849 (2016).
- [24] Y. Wu, W. Xia, W. Gao, F. Jia, P. Zhang, and W. Ren, Quasiparticle electronic structure of honeycomb C3N: from monolayer to bulk, *2D Mater.* **6**, 015018 (2018).
- [25] W. Gao, W. Xia, Y. Wu, W. Ren, X. Gao, and P. Zhang, Quasiparticle band structures of CuCl, CuBr, AgCl, and AgBr: The extreme case, *Phys. Rev. B* **98**, 045108 (2018).
- [26] W. Xia, W. Gao, G. Lopez-Candales, Y. Wu, W. Ren, W. Zhang, and P. Zhang, Combined subsampling and analytical integration for efficient large-scale GW calculations for 2D systems, *npj Comput. Mater.* **6**, 118 (2020).
- [27] J. P. Perdew, K. Burke, and M. Ernzerhof, Generalized gradient approximation made simple, *Phys. Rev. Lett.* **77**, 3865 (1996).
- [28] N. Troullier and J. L. Martins, Efficient pseudopotentials for plane-wave calculations, *Phys. Rev. B* **43**, 1993 (1991).
- [29] See Supplemental Material at <http://link.aps.org/supplemental/10.1103/PhysRevApplied.21.054019> for more details about the convergence test of the *GW* plus BSE calculations, the dependence of the electron density distribution and exciton radius on the choice of the hole position, and the *k*-resolved *e-h* pair amplitude plots.
- [30] N. C. Fernelius, Properties of gallium selenide single crystal, *Prog. Cryst. Growth Charact. Mater.* **28**, 275 (1994).
- [31] v. K. Schubert, E. Dorre, and M. Kluge, Zur kristallchemie der B-metalle. 3. kristallstruktur von GaSe und InTe, *Z. Metallkd.* **46**, 216 (1955).
- [32] D. Rybkovskiy, N. Arutyunyan, A. Orekhov, I. Gromchenko, I. Vorobiev, A. Osadchy, E. Y. Salaev, T. Baykara, K. Allakhverdiev, and E. Obraztsova, Size-induced effects in gallium selenide electronic structure: The influence of interlayer interactions, *Phys. Rev. B* **84**, 085314 (2011).
- [33] F. Li, X. Zhou, W. Feng, B. Fu, and Y. Yao, Thickness-dependent magneto-optical effects in hole-doped GaS and

- GaSe multilayers: A first-principles study, *New J. Phys.* **20**, 043048 (2018).
- [34] W. Feng, G.-Y. Guo, and Y. Yao, Tunable magneto-optical effects in hole-doped group-IIIA metal-monochalcogenide monolayers, *2D Mater.* **4**, 015017 (2016).
- [35] Z. B. Aziza, V. Zólyomi, H. Henck, D. Pierucci, M. G. Silly, J. Avila, S. J. Magorrian, J. Chaste, C. Chen, and M. Yoon, Valence band inversion and spin-orbit effects in the electronic structure of monolayer GaSe, *Phys. Rev. B* **98**, 115405 (2018).
- [36] G. Antonius, D. Y. Qiu, and S. G. Louie, Orbital symmetry and the optical response of single-layer MX monochalcogenides, *Nano Lett.* **18**, 1925 (2018).
- [37] R. Sporken, R. Hafsi, F. Coletti, J.-M. Debever, P. Thiry, and A. Chevy, Inverse-photoemission spectroscopy of GaSe and InSe, *Phys. Rev. B* **49**, 11093 (1994).
- [38] F. Coletti, R. Hafsi, J. Debever, and A. Chevy, Inverse photoemission of GaSe, *J. Lumin.* **48**, 645 (1991).
- [39] C. Depersinge, Absorption and electroabsorption near the indirect edge of GaSe, *Solid State Commun.* **21**, 317 (1977).
- [40] E. Cannuccia, B. Monserrat, and C. Attaccalite, Theory of phonon-assisted luminescence in solids: Application to hexagonal boron nitride, *Phys. Rev. B* **99**, 081109 (2019).
- [41] S. Brem, A. Ekman, D. Christiansen, F. Katsch, M. Selig, C. Robert, X. Marie, B. Urbaszek, A. Knorr, and E. Malic, Phonon-assisted photoluminescence from indirect excitons in monolayers of transition-metal dichalcogenides, *Nano Lett.* **20**, 2849 (2020).
- [42] L. Sponza, H. Amara, C. Attaccalite, S. Latil, T. Galvani, F. Paleari, L. Wirtz, and F. Ducastelle, Direct and indirect excitons in boron nitride polymorphs: A story of atomic configuration and electronic correlation, *Phys. Rev. B* **98**, 125206 (2018).
- [43] R. Le Toullec, N. Piccioli, and J. Chervin, Optical properties of the band-edge exciton in GaSe crystals at 10 K, *Phys. Rev. B* **22**, 6162 (1980).
- [44] V. V. Zalamai, N. N. Syrbu, I. G. Stamov, and S. I. Beril, Wannier–Mott excitons in GaSe single crystals, *J. Opt.* **22**, 085402 (2020).
- [45] A. Bosacchi, B. Bosacchi, and S. Franchi, Polariton effects in the exciton absorption of GaSe, *Phys. Rev. Lett.* **36**, 1086 (1976).
- [46] M. Stankovski, G. Antonius, D. Waroquiers, A. Miglio, H. Dixit, K. Sankaran, M. Giantomassi, X. Gonze, M. Côté, and G. M. Rignanese,  $G^0W^0$  band gap of ZnO: Effects of plasmon-pole models, *Phys. Rev. B* **84**, 241201 (2011).
- [47] P. Larson, M. Dvorak, and Z. Wu, Role of the plasmon-pole model in the  $GW$  approximation, *Phys. Rev. B* **88**, 125205 (2013).
- [48] B. C. Shih, Y. Xue, P. H. Zhang, M. L. Cohen, and S. G. Louie, Quasiparticle band gap of ZnO: High accuracy from the conventional  $G^0W^0$  approach, *Phys. Rev. Lett.* **105**, 146401 (2010).
- [49] G. Lopez-Candales, Z. Tang, W. Xia, F. Jia, and P. Zhang, Quasiparticle band structure of SrTiO<sub>3</sub> and BaTiO<sub>3</sub>: A combined LDA +  $U$  and  $G^0W^0$  approach, *Phys. Rev. B* **103**, 035128 (2021).
- [50] S. Adachi and Y. Shindo, Optical constants of  $\epsilon$ -GaSe, *J. Appl. Phys.* **71**, 428 (1992).
- [51] A. Budweg, D. Yadav, A. Grupp, A. Leitenstorfer, M. Trushin, F. Pauly, and D. Brida, Control of excitonic absorption by thickness variation in few-layer GaSe, *Phys. Rev. B* **100**, 045404 (2019).
- [52] M. Usman, S. Golovynskyi, D. Dong, Y. Lin, Z. Yue, M. Imran, B. Li, H. Wu, and L. Wang, Raman scattering and exciton photoluminescence in few-layer GaSe: Thickness- and temperature-dependent behaviors, *J. Phys. Chem. C* **126**, 10459 (2022).
- [53] C. Attaccalite, M. Palummo, E. Cannuccia, and M. Grüning, Second-harmonic generation in single-layer monochalcogenides: A response from first-principles real-time simulations, *Phys. Rev. Mater.* **3**, 074003 (2019).
- [54] V. K. Dien, N. T. Han, W. Bang-Li, K. I. Lin, and M. F. Lin, Tuning of the electronic and optical properties of monolayer GaSe via strain, *Adv. Theory Simul.* **6**, 2200950 (2023).
- [55] Z. Tang, G. J. Cruz, Y. Wu, W. Xia, F. Jia, W. Zhang, and P. Zhang, Giant narrow-band optical absorption and distinctive excitonic structures of monolayer C<sub>3</sub>N and C<sub>3</sub>B, *Phys. Rev. Appl.* **17**, 034068 (2022).
- [56] Z. Tang, G. J. Cruz, F. Jia, Y. Wu, W. Xia, and P. Zhang, Stacking up electron-rich and electron-deficient monolayers to achieve extraordinary mid- to far-infrared excitonic absorption: Interlayer excitons in the C<sub>3</sub>B/C<sub>3</sub>N bilayer, *Phys. Rev. Appl.* **19**, 044085 (2023).
- [57] F. H. da Jornada, D. Y. Qiu, and S. G. Louie, Nonuniform sampling schemes of the Brillouin zone for many-electron perturbation-theory calculations in reduced dimensionality, *Phys. Rev. B* **95**, 035109 (2017).
- [58] F. A. Rasmussen, P. S. Schmidt, K. T. Winther, and K. S. Thygesen, Efficient many-body calculations for two-dimensional materials using exact limits for the screened potential: Band gaps of MoS<sub>2</sub>, h-BN, and phosphorene, *Phys. Rev. B* **94**, 155406 (2016).
- [59] L. Matthes, P. Gori, O. Pulci, and F. Bechstedt, Universal infrared absorbance of two-dimensional honeycomb group-IV crystals, *Phys. Rev. B* **87**, 035438 (2013).

*Correction:* Support information in the Acknowledgment section contained a typographical error and has been fixed.